www.sciencemag.org/content/359/6378/900/suppl/DC1

Supplementary Material for

Breakup of last glacial deep stratification in the South Pacific

Chandranath Basak,* Henning Fröllje, Frank Lamy, Rainer Gersonde, Verena Benz,
Robert F. Anderson, Mario Molina-Kescher, Katharina Pahnke

*Corresponding author. Email: cbasak@csub.edu

Published 23 February 2018, *Science* **359**, 900 (2017)
DOI: 10.1126/science.aao2473

This PDF file includes:

Materials and Methods

Sample material and processing

Cores PS75/073-2, PS75/059-2, PS75/056-1, and PS75/054-1 used in this study were recovered during RV Polarstern cruise ANT-XXVI/2 in the South Pacific in November 2009-January 2010 (*53*). Bulk sediment samples from core E11-2 were obtained from a pre-sampled archive at Lamont Doherty Earth Observatory of Columbia University. All PS75 samples were washed and size-fractionated at the Alfred-Wegener-Institute, Bremerhaven. All following sample processing was done at the University of Oldenburg. Sediment samples were freeze dried and wet sieved to obtain the >63 µm fraction. From the >125 µm and >250 µm fractions, fish teeth and broken fish bones (hereafter called 'fish debris') and foraminifera, respectively, were picked for Nd isotope analyses. The Nd isotope record of core PS75/056-1 is based entirely on fish debris, whereas that of core E11-2 is based entirely on foraminifera. All other cores (PS75/054-1, PS75/059-2, PS75/073-2) have combined fish debris-foraminifera ε_{Nd} records.

Fish debris were cleaned in multiple steps, involving ultrasonication in optima grade methanol and MilliQ water (Millipore, 18 MΩ). The samples were then treated with a 1:1 solution of H_2O_2 (30%) and MilliQ, followed by dissolution in a 1:1 mixture of HNO_3 and HCl and drydown under a laminar flow hood. The samples were finally re-dissolved in 0.5 mL of 1 N HNO_3 in preparation for column chemistry.

Mixed species of planktic foraminifera (>250 µm fraction) from cores PS75/054-1 and E11-2 were subjected to physical cleaning only, according to published protocols for 'unclean foraminifera' [e.g, (*22, 54*)]. Cleaning comprised multiple rinses and sonication in optima grade methanol, followed by multiple rinses in deionized water. Following this step, foraminifera were gently crushed between glass slides to break open the inner chamber before repeating the sonication and rinse steps. The cleaned foraminifera fragments were examined under a microscope to ensure that no clay fragments were left in the sample. Cleaned crushed foraminifera were dried and dissolved in <10% acetic acid for 5-10 min. The dissolved solution was centrifuged and the supernatant was dried down and re-dissolved in 1 N HNO_3. Samples from cores PS75/059-2 and PS75/073-2 contained highly fragile foraminifera tests, which were cleaned using a slightly modified cleaning and dissolution protocol following that published by Tachikawa *et al. (54)*. About 30 mg of uncrushed foraminifera were transferred to a 15 mL centrifuge tube containing 500 µL of ultrapure water, 800-1000 µL of 1 M acetic acid was added at 100-200 µL increments to slowly dissolve the foraminifera. The dissolution process was stopped before the entire sample went into solution in order to minimize the potential of attacking lithogenic particles. This resulted in a residue consisting of chamber fragments and lithogenic particles. The solution-particle mixture was centrifuged at 5000 rpm for 10 min, the supernatant transferred to a 1.5 mL centrifuge tube and centrifuged again at 1000 rpm for 10 min. The final supernatant was transferred to a clean Teflon beaker, dried and transferred to nitric form by drying in concentrated HNO_3 followed by 1 N HNO_3.

We digested the lithogenic particles in order to monitor the Nd isotope signature of these potential contaminating phases that might be attacked during dissolution of foraminiferal calcite. The particle residue was transferred to a clean Teflon beaker and digested using HNO_3, HCl and HF at 100-150°C. The final solution was dried and transferred to nitric form by drying in 1 N HNO_3.

Column Chemistry and Isotope Measurements

In preparation for isotope measurements, Nd from all archives was isolated and purified by two-step column chemistry following established methods (*55*). Briefly, rare earth elements (REE) were separated from major cations using Eichrom TRU-Spec resin (particle size 100-150 μm) and Nd was purified from other REE using Eichrom or TrisKem LN-Spec resin (particle size 50-100 μm) and 0.23-0.25 N HCl as eluent. The Nd fraction was completely dried and treated with a 1:1 mixture of H_2O_2 (30%) and concentrated HNO_3 to ensure breakdown of any organic compounds that may have leaked during column chemistry. The samples were finally brought up in 2% HNO_3 for isotope analysis using a ThermoScientific Neptune Plus multi-collector inductively coupled plasma mass-spectrometer (MC-ICP-MS) at the University of Oldenburg.

All samples were aspirated into the MC-ICP-MS using a 100 μl nebulizer via a Cetac Aridus II desolvating unit. Nitrogen was used in the desolvating unit in order to stabilize the signal and minimize oxide formation. Preamplifier gains were performed at the beginning of each measurement session. Nd isotope data were acquired in static mode with 0.8 sec integration time over 4 blocks of 12 cycles each. All measured $^{143}Nd/^{144}Nd$ ratios were corrected for mass bias using an exponential law and a $^{146}Nd/^{144}Nd$ natural ratio of 0.7219 (*56*). In general, the international standard JNdi-1 was analyzed every 3 samples and all reported $^{143}Nd/^{144}Nd$ ratios were normalized to a JNdi-1 value of 0.512115 (*57*) using the mean $^{143}Nd/^{144}Nd$ of the JNdi-1 measurements of each analytical session. Standards analyzed in the course of the study were always concentration-matched with the samples. The external reproducibility was separately calculated for each session using the analyses of JNdi-1 and was generally better than ±0.3 ε_{Nd} units (2σ). Propagated errors are reported from combined external reproducibility of the measuring session and individual sample error (internal run error, 2σ) (Tables S1-S3). The procedural blank was ≤13 pg Nd (n=22).

Age Models

The age models of our cores were established by tuning their benthic or planktic $\delta^{18}O$ records to those of the high-resolution core MD97-2120 from the Chatham Rise in the Southwest Pacific (*19, 20*) (Fig. 1). In order to account for updated ^{14}C-calendar age calibrations (*58*), reservoir ages (560 ± 40 years (Holocene), 1970 ± 390 years (late glacial, ~28.7 ka) (*59, 60*), revised age of the Kawakawa ash (*61*), and additional ^{14}C ages (*60*), we revised the age scale of core MD97-2120 (Table S4, Figure S1). Age models of the investigated cores (except PS75/054-1) were created by graphical correlation of benthic $\delta^{18}O$ (PS75/056-1, PS75/059-2, E11-2) and planktic $\delta^{18}O$ (PS75/073-2) to reference core MD97-2120 on its updated age scale using the software AnalySeries 2.0.8 (*62*). The resulting age models of our cores and the updated age model of reference core MD97-2120 are summarized in Table S4 and Figure S1 and are described in detail in the following paragraphs.

The age model of core PS75/056-1 is based on the correlation of the benthic $\delta^{18}O$ isotope record [measured on *Cibicidoides kullenbergi*, published in (*63*)] to the benthic $\delta^{18}O$ of core MD97-2120 (*20*). The age model is based on seven age tie points within the upper 100 cm, which corresponds to ages of <30 ka. Resulting sedimentation rates range from 2 to 12 cm/ka. Our age model is in good agreement with a published age model that is based on correlation to reference core PS75/059-2 using benthic $\delta^{18}O$, diatom abundances, Fe and $CaCO_3$ contents, and summer sea surface temperatures (*64*), showing differences of ≤1.6 ka in the deglacial part (10-25 ka), and thus have no bearing on the interpretations of our results. Thus, age model uncertainties alone cannot account for the difference in timing of ε_{Nd} change between PS75/056-1 (at 18.8 ka) and core PS75/059-2, where ε_{Nd} starts to decrease at 13.4 ka (Table S1).

The age model for core PS75/059-2 was created by correlation of benthic $\delta^{18}O$ [measured on *C. kullenbergi*, published in (*63*)] to the benthic $\delta^{18}O$ record of MD97-2120 (*20*). This age model is based on six age tie points and results in sedimentation rates of 1 to 4 cm/ka. The deglacial decrease in $\delta^{18}O$ is in good agreement with that of PS75/056-1. Good correlation of XRF Sr and Fe data from PS75/059-2 with those of MD97-2120 suggest that the age model is robust. Further, our age model is in good agreement with recently published age models that are based on XRF tuning (*7*) and radiocarbon dating (*64*) with age differences of ≤1.1 ka and ≤1.5 ka, respectively between 0-20 ka. The decrease in ε_{Nd} values (~13.4 ka) in our age model happens at the same time when applying the age model of Ronge et al. (*7*). The ε_{Nd} decrease occurs at a younger age (~12.5 ka) when the age model of Benz et al. (*64*) is applied. Thus, the delay in ε_{Nd} decrease in core PS75/059-2 compared to the remaining deep cores is robust and cannot be attributed to age model uncertainties.

The age model of core PS75/073-2 is based on correlation of the planktic $\delta^{18}O$ record (measured on *Neogloboquadrina pachyderma* sinistral (*64*) to planktic $\delta^{18}O$ (*Globigerina bulloides*) of core MD97-2120 (*19*). The resulting sedimentation rates range between 1 and 8 cm/ka. Our age model is in good agreement with a published age model of this core that is based on radiocarbon dates (*64*) and with a recently published age model of nearby core (PS75/072-4) that is based on radiocarbon ages and correlation of planktic $\delta^{18}O$ to the EDC ice core deuterium record (*65*). Further, these authors report similar sedimentations rates (~0.2 to 9.5 cm/ka) as we observe for core PS75/073-2 for the studied interval. During the last 20 ka, differences between the published (*64*) and our age model are ≤2.5 ka (late glacial) and ≤1.4 ka (rest of the deglacial and Holocene record). Age model uncertainties are smaller than the observed delay in ε_{Nd} change (PS75/59-2 and probably E11-2 compared to core PS75/073-2) in our time series records, and therefore have no bearing on the interpretation and conclusion of this study. However, age model uncertainty may explain the delay (~1.5 ka) in the early deglacial (W1) ε_{Nd} change in core PS75/073-1 compared to that of PS75/056-1.

In order to maintain consistency, a new age model for core E11-2 was created based on correlation of the benthic δ^{18}O record (*66*) to that of core MD97-2120 (*20*). Sedimentation rates derived from this age model range between 6 and 16 cm/ka. The age model shows good agreement with the age model of nearby core PS75/056-1. When compared to the published age model by Ninnemann and Charles (*66*), all intervals exhibit age differences of <1 ka (Figure S3A), which has no bearing on the overall conclusions of this study.

The age model of core PS75/054-1 is based on correlation to nearby core PS75/056-1 (see above). We used XRF core scanner records of rubidium (Rb) data (XRF core scanner of the Alfred Wegener Institute, Bremerhaven). Rubidium is a common element in the siliciclastic fraction of the sediment and is concentrated in the fine-grained fraction. Similar to other lithogenic elements, Rb originates mainly from dust input at both locations and should therefore show the same temporal variations in both cores. Due to high water contents of the opal-rich glacial sediments in core PS75/54-1, we used the XRF scans of the heavier element Rb which is less affected by pore water than the commonly used Fe scans. Moreover, the Rb record is unaffected by bottom water redox changes or other early diagenetic overprints. We chose to correlate the Rb scan of core PS75/054-1 to that of core PS75/056-1 instead of to MD97-2120 in order to account for differences in terrigenous sediment supply to the Southeast (primarily eolian) and Southwest Pacific (primarily fluvial). Our age model is created using six age tie points within the last 30 ka, which results in sedimentation rates of 6 to 24 cm/ka for the last 20 ka (Figure S2). To corroborate the good correlation in the glacial to Holocene part of our core, Figure S2 shows the alignment of XRF Rb data throughout the last 150 ka between cores PS75/056-1 and PS75/054-1 as well as the Sr XRF data of cores PS75/056-1 and PS75/054-1. Rubidium shows a similar pattern in both cores throughout the last glacial-interglacial cycle, and the robustness of the Rb-based alignment is confirmed by the excellent agreement of the Sr data that largely follow carbonate fluctuations in the two cores.

Overall, the age models for the cores (except PS75/054-1) are independently derived, but referenced to the same age model (MD97-2120), making them internally consistent. The age models match those of previously published age models of the same and nearby cores in the deglacial section in general within ≤1.6 ka [(*7, 64-66*), see detailed discussion above]. Thus, the age scales provide accurate relative ages between cores and the best achievable absolute ages.

In order to test if the observed delays in ε_{Nd} in cores E11-2 and PS75/059-2 compared to cores PS75/056-1 and PS75/073-2 are an artifact of age model tuning, we created age models for cores E11-2 and PS75/059-2 by tuning their ε_{Nd} records to core PS75/056-1 (Figure S3). Results show that when aligning ε_{Nd} to the reference core, benthic δ^{18}O of both cores shift towards older ages, significantly offsetting them from that of the reference core (PS75/056-1). Further, the resulting age models do not agree with previously published age models of these cores (*7, 64, 66*). Thus, we conclude that the observed delay in ε_{Nd} is a real feature of our records and is not due to age model uncertainties.

Supplementary Text

<u>Hydrography and core locations</u>

The Southern Ocean is dominated by the eastward flowing Antarctic Circumpolar Current (ACC) and the circum-Antarctic frontal system with the Subantarctic Front (SAF) to the north, the Southern AAC Front to the south, and the Antarctic Polar Front (APF) in between [e.g., (*47*)]. Deep water that upwells south of the APF feeds both Antarctic Bottom Water (AABW) formation close the Antarctic continent and Antarctic Intermediate and Mode Water formation north of the APF [e.g., (*36, 67*)]. In the South Pacific, the overall location of the SAF and the APF varies by ~5°, with a more northward position in the west and southward in the east [(*47*), Figure 1 of the main text]. The Southern Ocean's major water mass, the Circumpolar Deep Water (CDW), is subdivided into an upper and lower branch. Lower CDW (LCDW) is identified by a salinity maximum that is inherited from North Atlantic Deep Water (NADW) (*47, 68*). Upper CDW (UCDW) is typically identified as an oxygen minimum layer, which is derived from oxygen-depleted, nutrient-rich Indian Deep Water (IDW) and North Pacific Deep Water (NPDW) (*69*). Lower CDW and UCDW are transported into the North Pacific, where they are transformed to NPDW and return to the Southern Ocean in the East Pacific along the South American continent at 1500-3500 m water depth (*70*). North of the SAF, UCDW is centered at approximately 1500 m depth and LCDW covers depths below 2000 m.

Core PS75/073-2 (3234 m) from the central/southwest Pacific is bathed today by LCDW and located south of the modern APF. By virtue of its location in the center of the ACC (Figure 1 of the main text), this core offers the ideal opportunity to study the evolution of pure CDW over the last deglaciation. Southeast Pacific cores PS75/056-1, PS75/059-2, E11-2, and PS75/054-1 are all located north of the modern SAF i.e., north of the ACC core. Currently, cores PS75/056-1 (3581 m) and E11-2 (3109) are bathed by LCDW, but are located close to the LCDW/UCDW boundary with some influence of low-oxygen UCDW, particularly to core E11-2 (Figure 1 of the main text). Thus, these two cores are best fitted to monitor past changes in the mixing proportions between LCDW and UCDW. Based on salinity values, core PS75/059-2 (3613 m) also represents LCDW, but it is separated from the other cores by the East-Pacific Rise (EPR) and has significant influence of low-oxygen NPDW (Figure 1 of the main text). Below LCDW, northward spreading dense AABW that is formed in the Weddell Sea, Ross Sea, and along the Adélie Coast, covers the abyss around Antarctica. In the South Pacific, the expansion of Ross Sea Bottom Water (RSBW), the coldest and saltiest variety of AABW, is restricted by bottom topography to areas south of the Pacific-Antarctic Ridge (*71*). Mixture of RSWB with overlying LCDW leads to erosion of the typical hydrographic properties along its flowpath towards the southeast Pacific (*71*), which is also seen in the ε_{Nd} signatures [e.g., (*11*)]. Core PS75/054-1 (4085 m) is located at the deeper limit of LCDW and just north of the modern extent of RSBW (Figure 1 of the main text). Its proximity to the RSBW boundary is ideal to investigate past changes in RSBW. Together, the southeast Pacific cores (E11-2, PS75/056-1, PS75/054-1) define an approximate meridional depth transect that can track the evolution of the water mass structure in the Southern Ocean during the last deglaciation.

Neodymium isotopes as a water mass tracer

The neodymium isotope composition ($^{143}Nd/^{144}Nd$) is expressed in the ε_{Nd} notation and defined as $\varepsilon_{Nd} = [(^{143}Nd/^{144}Nd)_{sample}/(^{143}Nd/^{144}Nd)_{CHUR} - 1]*10{,}000$ where CHUR is the Chondritic Uniform Reservoir with $^{143}Nd/^{144}Nd = 0.512638$ (*72*). The heterogeneous distribution of ε_{Nd} on the continents [e.g., (*73*)] is imprinted to seawater by transport of Nd from the continents to the ocean through rivers, dust and interaction with margin sediments known as 'boundary exchange'. Together with the short residence time of Nd in the ocean of 300-1000 years (*74, 75*), seawater ε_{Nd} allows the tracing of water masses back to their source region (*13, 76, 77*).

In the modern ocean, NADW has an ε_{Nd} signature of -13.5 (*13*), whereas NPDW is more radiogenic with an ε_{Nd} signature of -3.5 (*14*). Circumpolar Deep Water as a mixture of NADW and NPDW has intermediate values [ε_{Nd} = -8 to -9; (*11, 12, 78*)]. Deep waters formed around Antarctica carry a distinct ε_{Nd} signal depending on the formation region, ranging from ε_{Nd} = -7 (RSBW) in the Pacific sector (*11, 78, 79*) to -9 in the Atlantic sector of the Southern Ocean (*12*). In the South Pacific and the Pacific sector of the Southern Ocean, the main water masses carry distinct seawater ε_{Nd} signatures [e.g., NPDW, CDW, RSBW; (*11, 78-80*)]. Thus, Nd isotopes are an ideal proxy to study the paleo-water column structure in the South Pacific.

In the past, as NADW supply diminished or ceased, the relative contribution of NPDW increased changing the mixing proportion and altering the ε_{Nd} of CDW (*33*). Implicit in this mechanism is the assumption that the end-member ε_{Nd} signatures of NADW and NPDW remained constant over the time that is considered. Temporal stability of end-member NADW and NPDW ε_{Nd} signatures for the last 2 Ma is well established [e.g., (*15, 39, 40, 81, 82*)]. Broadly, NADW is a mixture of water from the Labrador Sea ($\varepsilon_{Nd} \sim -17$) and Iceland-Scotland Overflow Water (ISOW, $\varepsilon_{Nd} \sim -8.2$) with very distinct and different ε_{Nd} signatures acquired through interaction with surrounding lithogenic material (*83*). It is often suggested that the proportion of Labrador Sea Water and ISOW in NADW might have been different in the past, however, a concurrent change in NADW's ε_{Nd} signature has not yet been definitively reported. For RSBW (and other AABW varieties) that are formed on the Antarctic shelf and therefore inherit the ε_{Nd} of the shelf sediments, a change in ε_{Nd} would be conceivable if the provenance and lithology of these shelf sediments would have changed substantially. Since the Ross Sea receives its sediments through glacier transport, a change on the timescales discussed here is unlikely. Thus, we assume that the RSBW end-member remained constant for the time window of our study.

Fish teeth and Fe-Mn oxide coatings on foraminifera and sediment particles capture the bottom water ε_{Nd} signature at the sediment water interface and do not lose that signal during subsequent burial in the sediment column [e.g., (*22, 84, 85*)]. These archives have been effectively used to extract pristine paleo-bottom water signatures and as a proxy to trace water masses in past oceans [e.g., (*11, 16, 22, 86*)].

Testing the reliability of sedimentary archives and the Nd isotope proxy in the South Pacific

One pre-requisite to interpret ε_{Nd} changes in relation to water mass mixing and ocean circulation changes is to ascertain the reliability of sedimentary archive-derived core-top ε_{Nd} values in reflecting overlying bottom waters. The ε_{Nd} values from the core-tops in the South Pacific region show excellent agreement with those of overlying and/or nearby bottom water masses that are already published (Figure S4). It has recently been shown that boundary exchange in the deep South Pacific is limited to locations directly above the mid-ocean ridge (*11*) and therefore boundary exchange is not an issue for our core sites. Further, contributions from pore water fluids, as suggested for the Oregon margin (*87*) seem very unlikely, as nearby seawater ε_{Nd} profiles show no significant increase of Nd concentrations towards the seafloor, in fact, Nd concentrations south of the Polar Front are almost constant with depth and hence show the least increase with water depth found anywhere in the Pacific so far (*11, 78*).

Recent studies using dissolved Nd isotopes indicate a potential influence of NPDW on the isotope composition of deep waters in the southeast Pacific (*11, 80*). Thus, we interpret paleo ε_{Nd} signatures of the southeast Pacific (cores PS75/056-1, PS75/059-2, E11-2) in the context of admixture of NPDW and South Pacific CDW. Core PS75/073-2 is situated along the western flank of the Pacific-Antarctic Ridge. The core-top ε_{Nd} signature of -8.3 matches the nearest deep water representing CDW [Figure S4; (*11*)]. We thus consider this core as a representative of pure CDW composition in the South Pacific, excluded from direct influence of NPDW.

Neodymium isotope values of contemporaneous fossil fish teeth and debris have been demonstrated to be identical (*85, 88*). Here, separate analyses of contemporaneous fossil fish teeth and fish debris from one interval in core PS75/073-2 show that these two archives record the same ε_{Nd} values within analytical uncertainty, confirming the previous results (Table S2). In order to check the reproducibility between fossil fish teeth within a single sample, two samples with abundant teeth material were divided into sub-samples and consequently analyzed for Nd isotopes. The Nd isotope results of the subsamples are in agreement within the analytical uncertainty (Table S2).

Mixed species of planktic foraminifera were analyzed in samples and/or cores where fish debris was absent or revealed high measurement errors as a result of low availability and subsequent low Nd concentrations. To achieve highest reliability of our foraminifera based ε_{Nd} results, a few of these analyses were underpinned by fossil fish debris values during the course of this study (Table S1). Foraminifera ε_{Nd} vs. fish teeth/debris ε_{Nd} from the same sample show agreement within analytical error and closely follow a 1:1 line independent of the applied cleaning protocol (Table S2, Figure S5). Further, true replicates of uncleaned foraminifera reveal ε_{Nd} values within error, demonstrating the reproducibility of the analysis (Table S2). Based on our results, it is reasonable to assume that ε_{Nd} derived from fossil fish debris and Fe-Mn oxide coatings on foraminifera both record past bottom water ε_{Nd} in the South Pacific.

Leftover clay and/or lithogenic particles in foraminifera chambers are considered as one of the main sources of contamination when using a foraminiferal archive for ε_{Nd} studies [e.g., (*89*)]. To test the extent of contamination from these clay particles in samples that were not physically cleaned, we measured the ε_{Nd} composition of the residual particles (mixture of lithogenic particles and some undissolved foraminiferal calcite) following dissolution of the samples (Table S3). The ε_{Nd} signatures in these residual particles are in general more radiogenic, with a constant offset by ~1-2 ε_{Nd} units from the corresponding foraminifera and fish teeth values (Figure S5, Tables S2, S3). Given this constant offset and the consistency between fish teeth and foraminifera ε_{Nd}, we rule out contaminating influence of lithogenic material on uncleaned foraminifera for our samples. Based on our results and on what has previously been reported for directly dissolved foraminifera (*90*), we suggest that physical cleaning of foraminifera can be avoided when incremental dissolution of foraminifera is applied; this is at least true for our study region in the South Pacific, however, this approach should be tested on a regional basis.

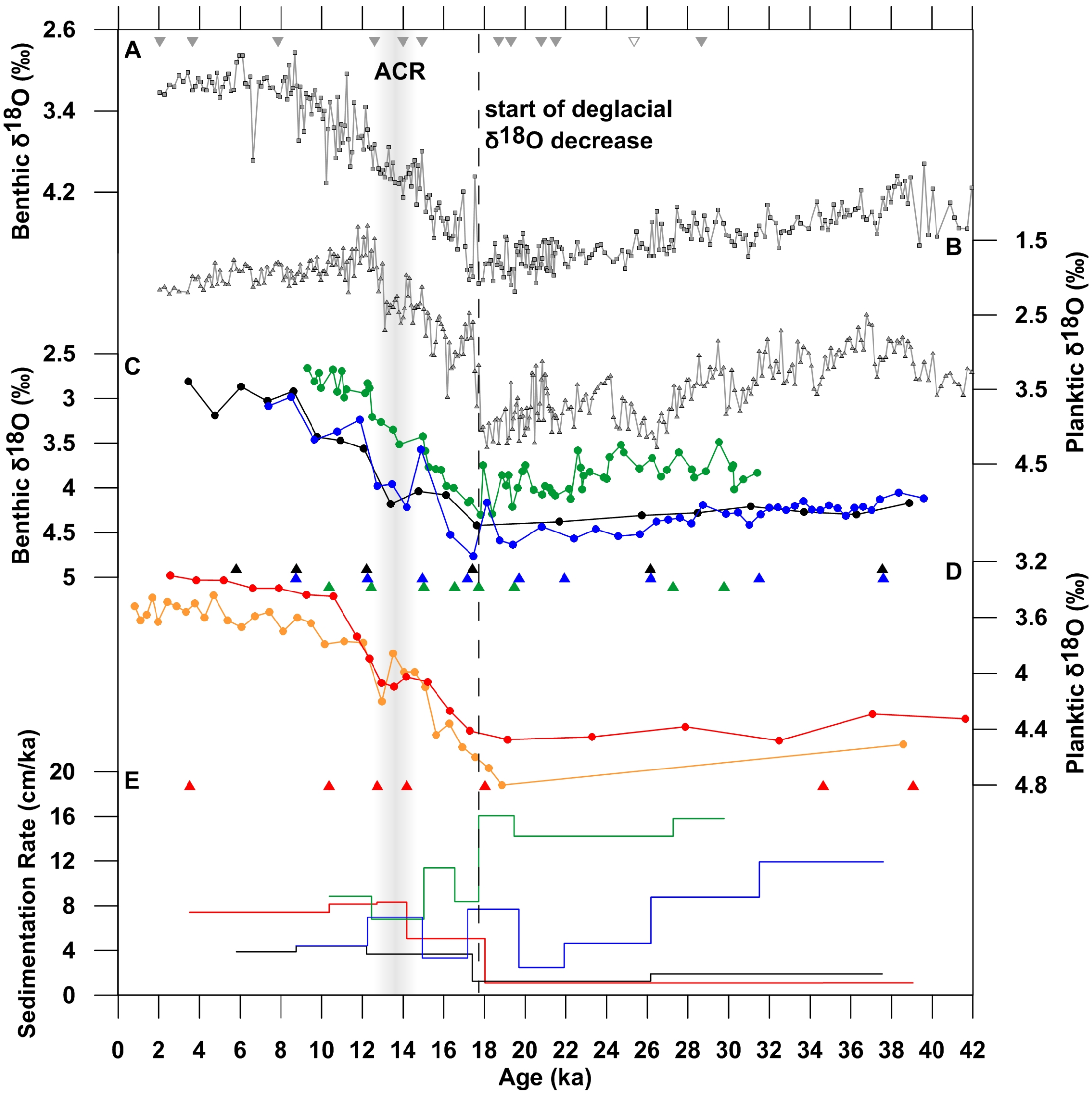

Fig. S1

Age model of investigated cores and reference core MD97-2120. A) Benthic $\delta^{18}O$ (*20*) and B) planktic $\delta^{18}O$ (*19*) of core MD97-2120 on the updated age scale. Grey filled triangles indicate ^{14}C-based tie points, open triangle indicates the Kawakawa Tephra tie point. C) Benthic $\delta^{18}O$ of cores PS75/056-1 (blue), PS75/059-2 (black) and E11-2 (green) aligned to MD97-2120. Benthic $\delta^{18}O$ of cores PS75/056-1 and PS75/059-2 from (*63*) and of E11-2 from (*66*). Triangles mark age tie points. D) Planktic $\delta^{18}O$ of core PS75/073-2 [red, (*64*)] aligned to MD97-2120 together with planktic $\delta^{18}O$ of nearby core PS75/072-4 [orange, (*65*)]. Red triangles are age tie points. E) Resulting sedimentation rates (colors as in C and D).

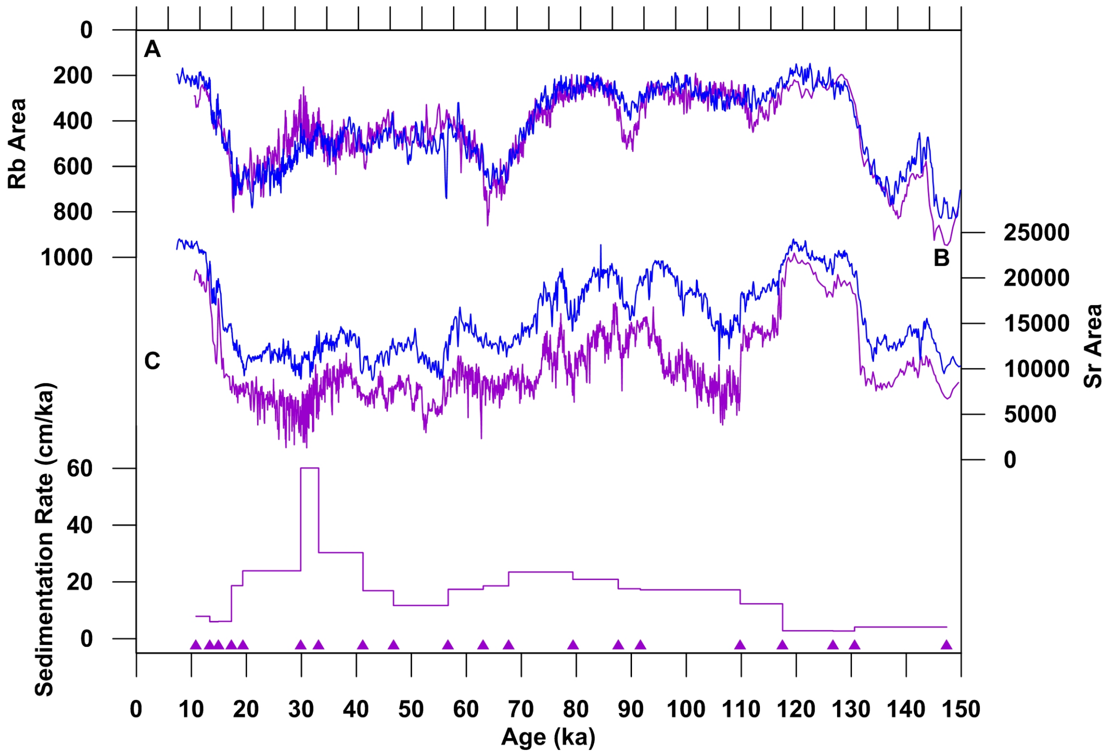

Fig. S2

A) Age model construction for core PS75/054-1 using XRF Rb data of core PS75/054-1 (purple) and aligning them to the Rb scan of core PS75/056-1 (blue) over the last 150 ka. B) XRF Sr scan of core PS75/054-1 on the Rb-based age model compared to XRF Sr data of PS75/056-1. C) Resulting sedimentation rate for PS75/054-1. Age tie points indicated by triangles. Note reversed y-axis in A).

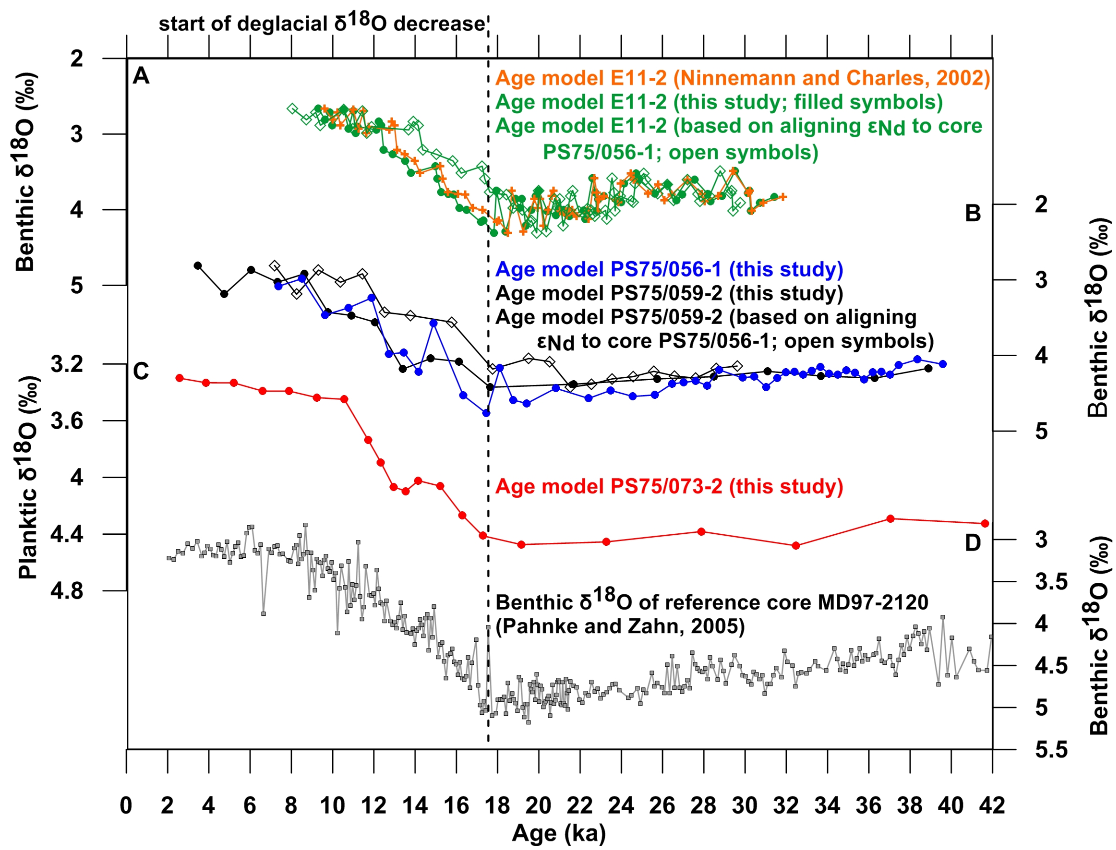

Fig. S3

Testing age model robustness. A) Comparison of benthic δ^{18}O record of core E11-2 on the age model used in this study (green) to a previously published age model [orange, (*66*)] and an age model constructed by aligning the timing of ε_{Nd} changes to those of core PS75/056-1 (open symbols). B) Benthic δ^{18}O records of PS75/056-1 (blue) and PS75/059-2 (black) on age models used in this study, and of PS75/059-2 (open symbols) on an age model constructed by aligning its ε_{Nd} record to that of PS75/056-1. The latter shows prominent disagreement in absolute δ^{18}O values to that of PS75/056-1, making this age model unrealistic. C) Planktic δ^{18}O record of PS75/073-2 on the age model used in this study. D) Benthic δ^{18}O record of core MD97-2120 (for details see Figure S1) plotted as a reference core to show the timing of change in the southern hemisphere. Age models of PS75/059-2 and E11-2, when tuned to the ε_{Nd} record of PS75/056-1 produce unrealistic patterns in their δ^{18}O records.

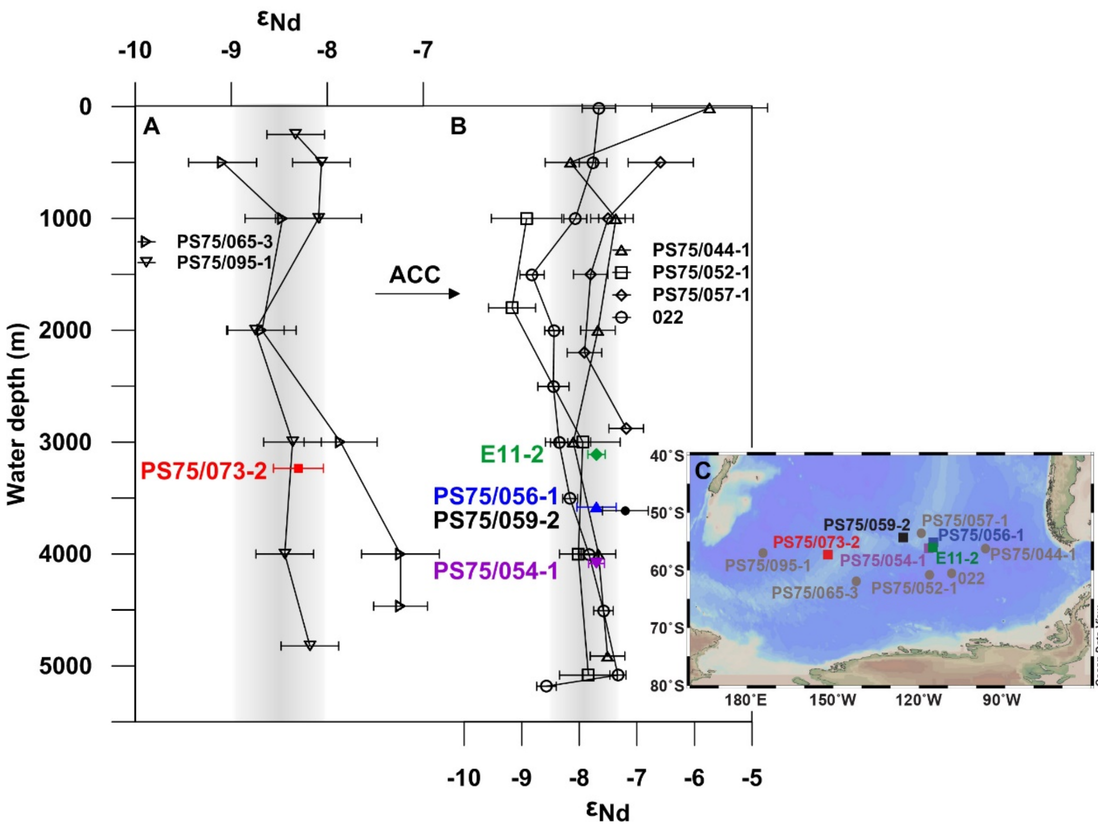

Fig. S4

Comparison of core-top foraminiferal or fish debris ε_{Nd} signatures (colored symbols) with water column profiles [black open symbols, (*11, 78*)] from A) the Western/Central and B) the Eastern South Pacific. Grey bars indicate range of ε_{Nd} for CDW. Bottom waters at site PS75/065-3 are influenced by RSBW (*11*). Arrow indicates general flow direction of the ACC, which becomes progressively more radiogenic from west to east, as expressed by increasing ε_{Nd} values of CDW. Seawater ε_{Nd} profiles from stations PS75/044-1, PS75/052-1, PS75/057-1, PS75/065-3, and PS75/095-1 from (*11*), data of station 022 from (*78*). C) Locations of sediment cores (colored) and seawater stations (grey) used in A) and B). Map created with Ocean Data View (*91*).

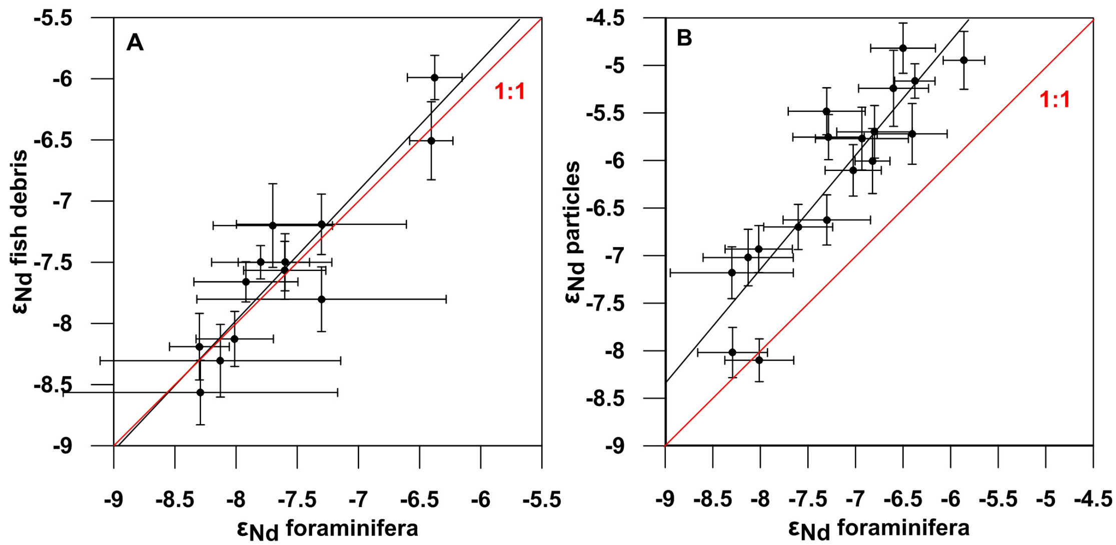

Fig. S5

ε_{Nd} values derived from foraminifera, fossil fish debris, and total digested silicate particles plotted in ε_{Nd}-ε_{Nd} space. A) Fish debris ε_{Nd} vs. foraminifera ε_{Nd} fall close to the ideal 1:1 line indicating fish debris and foraminifera archives can be used interchangeably. B) Total digested silicate particle ε_{Nd} vs. foraminifera ε_{Nd} exhibit a systematic offset of 1-2 epsilon units towards more radiogenic values in particles. The silicate particles used in these analyses were collected from inside the foraminifera tests collected during crushing and cleaning procedures. Detailed data presented in Tables S2 and S3.

Table S1.

Core information and composite ε_{Nd} records of all cores from this study.

Sample interval (cm)	Age (ka)	Material	Normalized $^{143}Nd/^{144}Nd$ [a]	ε_{Nd}	± Internal ε_{Nd} error (2σ SE)	± External ε_{Nd} error (2σ SD)	± Propagated error
E11-2-1, 56˚S, 115˚W, 3109 m							
21-22	9.13	foraminifera	0.512243	-7.7	0.08	0.13	0.15
26-27	9.70	foraminifera	0.512241	-7.7	0.14	0.13	0.19
41-42	11.39	foraminifera	0.512242	-7.7	0.02	0.13	0.13
43-44	11.62	foraminifera	0.512252	-7.5	0.12	0.13	0.18
44-45	11.73	foraminifera	0.512250	-7.6	0.17	0.22	0.28
53-54	12.84	foraminifera	0.512267	-7.2	0.07	0.13	0.15
60-61	13.88	foraminifera	0.512271	-7.2	0.22	0.13	0.26
72-73	15.39	foraminifera	0.512320	-6.2	0.20	0.24	0.31
74-75	15.57	foraminifera	0.512339	-5.8	0.09	0.23	0.25
76-77	15.74	foraminifera	0.512319	-6.2	0.16	0.23	0.28
83-84	16.36	foraminifera	0.512341	-5.8	0.08	0.13	0.15
84-85	16.45	foraminifera	0.512341	-5.8	0.15	0.13	0.20
85-86	16.53	foraminifera	0.512335	-5.9	0.22	0.13	0.26
86-87	16.65	foraminifera	0.512347	-5.7	0.12	0.22	0.25
93-94	17.49	foraminifera	0.512339	-5.8	0.19	0.22	0.29
103-104	18.22	foraminifera	0.512332	-6.0	0.11	0.22	0.25
137-138	20.45	foraminifera	0.512326	-6.1	0.12	0.22	0.25
144-145	20.94	foraminifera	0.512332	-6.0	0.11	0.22	0.25
145-146	21.01	foraminifera	0.512322	-6.2	0.15	0.22	0.27
146-147	21.08	foraminifera	0.512327	-6.1	0.11	0.22	0.25
152-153	21.51	foraminifera	0.512329	-6.0	0.17	0.22	0.28
155-156	21.72	foraminifera	0.512326	-6.1	0.21	0.22	0.30
156-157	21.79	foraminifera	0.512328	-6.0	0.07	0.22	0.23
157-158	21.86	foraminifera	0.512325	-6.1	0.16	0.22	0.27
164-165	22.35	foraminifera	0.512313	-6.3	0.16	0.22	0.27
165-166	22.42	foraminifera	0.512317	-6.3	0.02	0.22	0.22
176-177	23.19	foraminifera	0.512322	-6.2	0.08	0.22	0.23
195-196	24.53	foraminifera	0.512304	-6.5	0.10	0.22	0.24

PS75/073-2, 57°12.27'S, 151°36.63'W, 3234 m							
3-4	2.58	foraminifera	0.512213	-8.3	0.16	0.21	0.26
7.5-8.5	3.18	foraminifera	0.512227	-8.0	0.08	0.21	0.22
12.5-13.5	3.86	fish teeth/debris	0.512215	-8.3	0.06	0.31	0.32
22.5-23.5	5.20	fish debris/foram. [b]		-8.3	0.26	0.26	0.37
27.5-28.5	5.87	fish debris	0.512217	-8.2	0.18	0.29	0.34
33-34	6.61	fish debris	0.512211	-8.3	0.33	0.30	0.45
42.5-43.5	7.89	fish debris	0.512205	-8.4	0.39	0.29	0.49
52.5-53.5	9.24	foraminifera	0.512227	-8.0	0.13	0.21	0.25
57-58	9.84	foraminifera	0.512221	-8.1	0.21	0.21	0.30
62.5-63.5	10.56	fish teeth/debris	0.512234	-7.9	0.48	0.27	0.55
67.5-68.5	11.18	fish debris	0.512220	-8.2	0.08	0.29	0.30
72-73	11.73	fish teeth/debris	0.512226	-8.0	0.16	0.31	0.35
73-75	11.91	fish debris	0.512231	-7.9	0.32	0.23	0.39
75-76	12.10	fish debris	0.512230	-8.0	0.11	0.39	0.41
77-78	12.34	foraminifera	0.512248	-7.6	0.11	0.21	0.24
79-80	12.59	fish debris	0.512258	-7.4	0.20	0.23	0.30
82-83	12.95	foraminifera	0.512278	-7.0	0.17	0.21	0.27
84-85	13.19	foraminifera	0.512283	-6.9	0.19	0.27	0.33
87-88	13.55	fish teeth/debris	0.512291	-6.8	0.15	0.31	0.34
89-90	13.79	foraminifera	0.512288	-6.8	0.21	0.27	0.34
92-93	14.15	fish teeth/debris	0.512297	-6.7	0.16	0.29	0.33
94-95	14.52	fish debris	0.512285	-6.9	0.14	0.23	0.27
97.5-98.5	15.21	foraminifera	0.512296	-6.7	0.18	0.21	0.28
103-104	16.29	fish debris/foram. [b]		-6.5	0.27	0.24	0.36
104-105	16.49	fish teeth	0.512298	-6.6	0.31	0.33	0.45
108-109	17.28	fish debris/foram. [b]		-6.0	0.18	0.37	0.41
109-110	17.48	fish teeth/debris	0.512330	-6.0	0.13	0.18	0.22
113-114	19.14	fish teeth/debris	0.512326	-6.1	0.12	0.12	0.17
114-115	20.06	fish teeth	0.512320	-6.2	0.05	0.21	0.22
117.5-118.5	23.28	fish teeth	0.512328	-6.0	0.07	0.31	0.32
118-119	23.74	fish teeth	0.512325	-6.1	0.09	0.18	0.20
122.5-123.5	27.88	fish teeth [b]		-6.1	0.25	0.18	0.31
123.5-124.5	28.79	fish teeth	0.512328	-6.0	0.23	0.21	0.31

PS75/056-1, 55°09.74'S, 114°47.31'W, 3581 m							
0-1.5	7.38	fish debris	0.512243	-7.7	0.12	0.32	0.34
4.5-6	8.51	fish debris	0.512292	-6.7	0.48	0.32	0.58
9.5-11	9.63	fish debris	0.512229	-8.0	0.86	0.25	0.90
14.5-16	10.76	fish debris	0.512254	-7.5	0.67	0.34	0.75
19.5-21	11.89	fish debris	0.512247	-7.6	0.14	0.25	0.29
24.5-26	12.74	fish debris	0.512258	-7.4	0.24	0.25	0.35
29.5-31	13.45	fish debris	0.512293	-6.7	0.13	0.25	0.28
34.5-36	14.17	fish debris	0.512314	-6.3	0.16	0.25	0.30
39.5-41	14.89	fish debris	0.512294	-6.7	0.25	0.25	0.35
44.4-46 [c]	16.33	fish debris	0.512315	-6.3	0.36	0.20	0.41
49.5-51	17.46	fish debris	0.512329	-6.0	0.10	0.25	0.27
54.5-56	18.11	fish debris	0.512335	-5.9	0.26	0.25	0.36
59.5-61	18.76	fish debris	0.512353	-5.6	0.03	0.23	0.23
64.5-66	19.41	fish debris	0.512347	-5.7	0.16	0.23	0.28
69.5-71	20.82	fish debris	0.512351	-5.6	0.22	0.23	0.32
74.5-76	22.41	fish debris	0.512331	-6.0	0.28	0.23	0.36
79.5-81	23.48	fish debris	0.512328	-6.0	0.31	0.23	0.39
84.5-86	24.56	fish debris	0.512330	-6.0	0.14	0.13	0.19
89.5-91	25.63	fish debris	0.512314	-6.3	0.22	0.18	0.28
94.5-96	26.45	fish debris	0.512311	-6.4	0.11	0.25	0.27
99.5-101	27.02	fish debris	0.512286	-6.9	0.36	0.25	0.44
104.5-106	27.59	fish debris	0.512313	-6.3	0.15	0.27	0.31
114.5-116	28.73	fish debris	0.512325	-6.1	0.10	0.27	0.29
124.5-126	29.87	fish debris	0.512315	-6.3	0.30	0.23	0.38
PS75/059-2, 54°12.80'S, 125°25.53'W, 3613 m							
2-3	3.46	fish debris	0.512270	-7.2	0.26	0.30	0.40
7-8	4.75	fish debris	0.512282	-6.9	0.09	0.28	0.29
12-13	6.04	foraminifera	0.512264	-7.3	0.16	0.21	0.26
17-18	7.33	foraminifera	0.512265	-7.3	0.11	0.21	0.24
22-23	8.62	foraminifera	0.512264	-7.3	0.13	0.21	0.25
27.28	9.78	fish debris	0.512276	-7.1	0.22	0.28	0.36
32.33	10.92	fish debris	0.512284	-6.9	0.07	0.28	0.29
37-38	12.06	foraminifera [b]		-6.6	0.38	0.30	0.48
42-43	13.40	fish teeth/debris	0.512342	-5.8	0.14	0.27	0.30

47-48	14.76	fish teeth/debris	0.512346	-5.7	0.13	0.20	0.24
52-53	16.12	fish teeth/debris	0.512345	-5.7	0.16	0.20	0.26
57-58	17.63	foraminifera	0.512338	-5.9	0.22	0.21	0.30
62-63	21.68	fish teeth/debris	0.512341	-5.8	0.42	0.27	0.50
67-68	25.73	fish teeth	0.512329	-6.0	0.30	0.30	0.42
72-73	28.48	fish teeth/debris	0.512321	-6.2	0.21	0.30	0.37
PS75/054-1, 56°9.105'S, 115°7.982'W, 4085 m							
17.5-19	12.91	foraminifera	0.512245	-7.7	0.04	0.13	0.14
22.5-24	13.45	fish debris	0.512325	-6.1	0.10	0.32	0.34
27.5-29	14.27	fish debris/foram. [b]		-7.8	0.30	0.35	0.46
32.5-34	15.05	fish debris	0.512304	-6.5	0.42	0.32	0.53
37.5-39	15.99	fish debris/foram. [b]		-7.5	0.49	0.35	0.60
47.5-49	17.41	fish debris/foram. [b]		-7.7	0.32	0.27	0.42
57.5-59	17.93	fish debris/foram. [b]		-7.6	0.21	0.39	0.45
67.5-69	18.45	foraminifera	0.512257	-7.4	0.15	0.23	0.27
87.5-89	19.41	foraminifera	0.512276	-7.1	0.13	0.13	0.18

[a] Sample $^{143}Nd/^{144}Nd$ ratios measured by MC-ICP-MS were normalized to the mean of JNdi-1 of the particular analytical session, relative to a JNdi-1 value of 0.512115 (*57*)
[b] Average of two individual measurements (fish teeth, fish debris, foraminifera) from the same sample. Individual results in Table S2
[c] Sample analyzed at Helmholtz Institute for Marine Research, Geomar, Kiel (Germany).

Table S2.

Data of individual analyses of fish teeth/debris and foraminifera.

Sample interval (cm)	Age (ka)	Material	Normalized $^{143}Nd/^{144}Nd$	ε_{Nd}	± Internal ε_{Nd} error (2σ SE)	± External ε_{Nd} error (2σ SD)	± Propagated error
PS75/073-2, 57°12.27'S, 151°36.63'W, 3234 m							
3-4	2.58	fish teeth/debris	0.512199	-8.6	0.86	0.72	1.12
3-4	2.58	foraminifera	0.512213	-8.3	0.16	0.21	0.26
7.5-8.5	3.18	fish debris	0.512221	-8.1	0.10	0.30	0.32
7.5-8.5	3.18	foraminifera	0.512227	-8.0	0.08	0.21	0.22
22.5-23.5	5.20	fish debris	0.512218	-8.2	0.14	0.20	0.24
22.5-23.5	5.20	foraminifera	0.512211	-8.3	0.22	0.16	0.27
52.5-53.5	9.24	fish debris [a]	0.512335	-5.9	0.98	0.27	1.02
52.5-53.5	9.24	foraminifera	0.512227	-8.0	0.13	0.21	0.25
57-58	9.84	fish debris [a]	0.512212	-8.3	0.67	0.72	0.98
57-58	9.84	foraminifera	0.512221	-8.1	0.21	0.21	0.30
77-78	12.34	fish debris [a]	0.512250	-7.6	0.17	0.29	0.34
77-78	12.34	foraminifera	0.512248	-7.6	0.11	0.21	0.24
89-90	13.79	fish teeth/debris [a]	0.512261	-7.4	0.41	0.33	0.53
89-90	13.79	foraminifera	0.512288	-6.8	0.21	0.27	0.34
103-104	16.29	fish debris	0.512304	-6.5	0.13	0.12	0.18
103-104	16.29	foraminifera	0.512310	-6.4	0.24	0.21	0.32
108-109	17.28	fish debris	0.512324	-6.1	0.07	0.20	0.21
108-109	17.28	fish teeth	0.512335	-5.9	0.17	0.31	0.35
122.5-123.5	27.88	fish teeth	0.512328	-6.0	0.22	0.12	0.25
122.5-123.5	27.88	fish teeth	0.512324	-6.1	0.12	0.13	0.18
127.5-128.5	32.47	fish teeth [b]	0.512314	-6.3	0.19	0.12	0.22
127.5-128.5	32.47	fish teeth [b]	0.512335	-5.9	0.17	0.12	0.21
PS75/059-2, 54°12.80'S, 125°25.53'W, 3613 m							
12-13	6.04	fish debris [a]	0.512238	-7.8	0.98	0.28	1.02
12-13	6.04	foraminifera	0.512264	-7.3	0.16	0.21	0.26
22-23	8.62	fish debris [a]	0.512269	-7.2	0.64	0.27	0.69
22-23	8.62	foraminifera	0.512264	-7.3	0.13	0.21	0.25
37-38	12.06	foraminifera	0.512298	-6.6	0.34	0.21	0.40
37-38	12.06	foraminifera	0.512303	-6.5	0.16	0.21	0.26

77-78	31.08	fish debris [b]	0.512331	-6.0	0.10	0.20	0.22
77-78	31.08	foraminifera [b]	0.512311	-6.4	0.02	0.18	0.18
PS75/054-1, 56°9.105'S, 115°7.982'W, 4085 m							
27.5-29	14.27	fish debris	0.512246	-7.6	0.28	0.32	0.43
27.5-29	14.27	foraminifera	0.512232	-7.9	0.10	0.13	0.16
37.5-39	15.99	fish debris	0.512269	-7.2	0.47	0.13	0.49
37.5-39	15.99	foraminifera	0.512241	-7.7	0.12	0.32	0.34
47.5-49	17.41	fish debris	0.512253	-7.5	0.32	0.24	0.40
47.5-49	17.41	foraminifera	0.512238	-7.8	0.04	0.13	0.14
57.5-59	17.93	fish debris	0.512253	-7.5	0.21	0.32	0.38
57.5-59	17.93	foraminifera	0.512247	-7.6	0.04	0.23	0.23

[a] Values used in supplementary figures for archive- or replicate-comparison. These values are excluded from the composite record (Table S1) due to higher error or low voltage during measurement

[b] Values used in supplementary figures for archive- or replicate-comparison but not included in the composite records due to ages >30 ka (Table S1).

Table S3.

Data of individual analyses of lithogenic particles from inside foraminifera shells.

Sample interval (cm)	Age (ka)	Normalized $^{143}Nd/^{144}Nd$	ε_{Nd}	± Internal ε_{Nd} error (2σ SE)	± External ε_{Nd} error (2σ SD)	± Propagated error
PS75/073-2, 57°12.27'S, 151°36.63'W, 3234 m						
3-4	2.58	0.512229	-8.0	0.16	0.33	0.37
7.5-8.5	3.18	0.512221	-8.1	0.15	0.33	0.36
22.5-23.5	5.20	0.512270	-7.2	0.34	0.55	0.65
52.5-53.5	9.24	0.512283	-6.9	0.24	0.26	0.35
57-58	9.84	0.512280	-7.0	0.34	0.33	0.47
77-78	12.34	0.512297	-6.7	0.15	0.33	0.36
82-83	12.95	0.512325	-6.1	0.14	0.26	0.30
84-85	13.19	0.512342	-5.8	0.33	0.36	0.49
89-90	13.79	0.512332	-6.0	0.09	0.16	0.18
97.5-98.5	15.21	0.512346	-5.7	0.30	0.26	0.40
103-104	16.29	0.512345	-5.7	0.26	0.26	0.37
PS75/059-2, 54°12.80'S, 125°25.53'W, 3613 m						
12-13	6.04	0.512301	-6.6	0.32	0.33	0.46
17-18	7.33	0.512343	-5.8	0.27	0.26	0.37
22-23	8.62	0.512357	-5.5	0.31	0.26	0.40
37-38	12.06	0.512369	-5.2	0.26	0.26	0.37
37-38	12.06	0.512391	-4.8	0.22	0.26	0.34
57-58	17.63	0.512384	-5.0	0.06	0.21	0.22
77-78	31.08	0.512373	-5.2	0.03	0.21	0.21

Table S4.

Updated age model tie points of reference core MD97-2120 and tie points of the investigated cores

Core	Sample interval (cm)	Age (ka)	Type	Sed. Rate (cm/ka)	Data Reference
MD97-2120	22.5	2.06	^{14}C	8.8	(*19*)
	36.5	3.66	^{14}C	14.8	(*19*)
	98.5	7.86	^{14}C	21.9	(*19*)
	202.5	12.61	^{14}C	20.3	(*19*)
	230.5	13.99	^{14}C	23.7	(*19*)
	252.5	14.92	^{14}C	20.6	(*19*)
	330.5	18.7	^{14}C	23.3	(*60*)
	344.5	19.3	^{14}C	30.7	(*60*)
	390.5	20.8	^{14}C	39.3	(*60*)
	418	21.5	^{14}C	13.7	(*60*)
	471	25.36	Kawakawa Tephra	16.3	(*61*)
	525	28.67	^{14}C	14.8	(*19*)
E11-2	32.5	10.37	Benthic $\delta^{18}O$	8.8	(*66*)
	50.8	12.44	Benthic $\delta^{18}O$	6.8	(*66*)
	68.3	15.02	Benthic $\delta^{18}O$	11.4	(*66*)
	85.6	16.54	Benthic $\delta^{18}O$	8.4	(*66*)
	95.5	17.72	Benthic $\delta^{18}O$	16.1	(*66*)
	123.4	19.46	Benthic $\delta^{18}O$	14.2	(*66*)
	234.5	27.27	Benthic $\delta^{18}O$	15.8	(*66*)
	274.2	29.78	Benthic $\delta^{18}O$		(*66*)
PS75/073-2	10.5	3.52	Planktic $\delta^{18}O$	7.4	(*64*)
	61.4	10.37	Planktic $\delta^{18}O$	8.2	(64)
	80.7	12.73	Planktic $\delta^{18}O$	8.3	(64)
	92.8	14.19	Planktic $\delta^{18}O$	5.1	(64)
	112.3	18.02	Planktic $\delta^{18}O$	1.1	(64)
	130.4	34.64	Planktic $\delta^{18}O$	1.1	(64)
	135.2	39.06	Planktic $\delta^{18}O$		(64)

PS75/056-1	6.6	8.74	Benthic $\delta^{18}O$	4.4	(*63*)
	22.1	12.25	Benthic $\delta^{18}O$	7.0	(63)
	40.9	14.95	Benthic $\delta^{18}O$	3.3	(63)
	48.3	17.17	Benthic $\delta^{18}O$	7.7	(63)
	67.7	19.69	Benthic $\delta^{18}O$	2.5	(63)
	73.3	21.93	Benthic $\delta^{18}O$	4.7	(63)
	93.0	26.17	Benthic $\delta^{18}O$	8.8	(63)
	139.8	31.51	Benthic $\delta^{18}O$	11.9	(63)
	212.4	37.60	Benthic $\delta^{18}O$		(63)
PS75/059-2	11.6	5.81	Benthic $\delta^{18}O$	3.9	(63)
	23.0	8.75	Benthic $\delta^{18}O$	4.4	(63)
	38.1	12.20	Benthic $\delta^{18}O$	3.7	(63)
	57.2	17.41	Benthic $\delta^{18}O$	1.2	(63)
	68.0	26.16	Benthic $\delta^{18}O$	1.9	(63)
	89.9	37.55	Benthic $\delta^{18}O$		(63)
PS75/054-1	15.8	10.82	XRF Rb	7.9	
	29.7	13.34	XRF Rb	6.0	
	40.6	14.90	XRF Rb	6.1	
	49.2	17.29	XRF Rb	18.7	
	64.9	19.33	XRF Rb	23.9	
	125.5	29.87	XRF Rb	60.1	
	159.3	33.14	XRF Rb	30.3	
	227.1	41.20	XRF Rb	16.9	
	249.8	46.75	XRF Rb	11.7	
	290.6	56.70	XRF Rb	17.4	
	319.3	63.07	XRF Rb	18.6	
	341.5	67.70	XRF Rb	23.5	
	414.1	79.37	XRF Rb	20.9	
	478.0	87.62	XRF Rb	17.6	
	497.8	91.65	XRF Rb	17.2	
	594.8	109.80	XRF Rb	12.3	
	633.8	117.52	XRF Rb	2.8	
	680.6	126.70	XRF Rb	2.7	
	697.0	130.60	XRF Rb	4.1	

761.4	147.36	XRF Rb

References and Notes

1. F. Parrenin, V. Masson-Delmotte, P. Köhler, D. Raynaud, D. Paillard, J. Schwander, C. Barbante, A. Landais, A. Wegner, J. Jouzel, Synchronous change of atmospheric CO_2 and Antarctic temperature during the last deglacial warming. *Science* **339**, 1060–1063 (2013). doi:10.1126/science.1226368 Medline

2. D. M. Sigman, E. A. Boyle, Glacial/interglacial variations in atmospheric carbon dioxide. *Nature* **407**, 859–869 (2000). doi:10.1038/35038000 Medline

3. D. M. Sigman, M. P. Hain, G. H. Haug, The polar ocean and glacial cycles in atmospheric $CO(_2)$ concentration. *Nature* **466**, 47–55 (2010). doi:10.1038/nature09149 Medline

4. A. Abelmann, R. Gersonde, G. Knorr, X. Zhang, B. Chapligin, E. Maier, O. Esper, H. Friedrichsen, G. Lohmann, H. Meyer, R. Tiedemann, The seasonal sea-ice zone in the glacial Southern Ocean as a carbon sink. *Nat. Commun.* **6**, 8136 (2015). doi:10.1038/ncomms9136 Medline

5. R. F. Anderson, S. Ali, L. I. Bradtmiller, S. H. H. Nielsen, M. Q. Fleisher, B. E. Anderson, L. H. Burckle, Wind-driven upwelling in the Southern Ocean and the deglacial rise in atmospheric CO_2. *Science* **323**, 1443–1448 (2009). doi:10.1126/science.1167441 Medline

6. A. Burke, L. F. Robinson, The Southern Ocean's role in carbon exchange during the last deglaciation. *Science* **335**, 557–561 (2012). doi:10.1126/science.1208163 Medline

7. T. A. Ronge, R. Tiedemann, F. Lamy, P. Köhler, B. V. Alloway, R. De Pol-Holz, K. Pahnke, J. Southon, L. Wacker, Radiocarbon constraints on the extent and evolution of the South Pacific glacial carbon pool. *Nat. Commun.* **7**, 11487 (2016). doi:10.1038/ncomms11487 Medline

8. I. N. McCave, L. Carter, I. R. Hall, Glacial–interglacial changes in water mass structure and flow in the SW Pacific Ocean. *Quat. Sci. Rev.* **27**, 1886–1908 (2008). doi:10.1016/j.quascirev.2008.07.010

9. E. L. Sikes, M. S. Cook, T. P. Guilderson, Reduced deep ocean ventilation in the Southern Pacific Ocean during the last glaciation persisted into the deglaciation. *Earth Planet. Sci. Lett.* **438**, 130–138 (2016). doi:10.1016/j.epsl.2015.12.039

10. R. Ferrari, M. F. Jansen, J. F. Adkins, A. Burke, A. L. Stewart, A. F. Thompson, Antarctic sea ice control on ocean circulation in present and glacial climates. *Proc. Natl. Acad. Sci. U.S.A.* **111**, 8753–8758 (2014). doi:10.1073/pnas.1323922111 Medline

11. C. Basak, K. Pahnke, M. Frank, F. Lamy, R. Gersonde, Neodymium isotopic characterization of Ross Sea Bottom Water and its advection through the southern South Pacific. *Earth Planet. Sci. Lett.* **419**, 211–221 (2015). doi:10.1016/j.epsl.2015.03.011

12. T. Stichel, M. Frank, J. Rickli, B. A. Haley, The hafnium and neodymium isotope composition of seawater in the Atlantic sector of the Southern Ocean. *Earth Planet. Sci. Lett.* **317-318**, 282–294 (2012). doi:10.1016/j.epsl.2011.11.025

13. F. Lacan, C. Jeandel, Acquisition of the neodymium isotopic composition of the North Atlantic Deep Water. *Geochem. Geophys. Geosyst.* **6**, Q12008 (2005). doi:10.1029/2005GC000956

14. H. Fröllje, K. Pahnke, B. Schnetger, H.-J. Brumsack, H. Dulai, J. N. Fitzsimmons, Hawaiian imprint on dissolved Nd and Ra isotopes and rare earth elements in the central North Pacific: Local survey and seasonal variability. *Geochim. Cosmochim. Acta* **189**, 110–131 (2016). doi:10.1016/j.gca.2016.06.001

15. L. D. Pena, S. L. Goldstein, Thermohaline circulation crisis and impacts during the mid-Pleistocene transition. *Science* **345**, 318–322 (2014). doi:10.1126/science.1249770 Medline

16. A. M. Piotrowski, S. L. Goldstein, S. R. Hemming, R. G. Fairbanks, Intensification and variability of ocean thermohaline circulation through the last deglaciation. *Earth Planet. Sci. Lett.* **225**, 205–220 (2004). doi:10.1016/j.epsl.2004.06.002

17. L. C. Skinner, A. E. Scrivner, D. Vance, S. Barker, S. Fallon, C. Waelbroeck, North Atlantic versus Southern Ocean contributions to a deglacial surge in deep ocean ventilation. *Geology* **41**, 667–670 (2013). doi:10.1130/G34133.1

18. J. Lippold, M. Gutjahr, P. Blaser, E. Christner, M. L. de Carvalho Ferreira, S. Mulitza, M. Christl, F. Wombacher, E. Böhm, B. Antz, O. Cartapanis, H. Vogel, S. L. Jaccard, Deep water provenance and dynamics of the (de)glacial Atlantic meridional overturning circulation. *Earth Planet. Sci. Lett.* **445**, 68–78 (2016). doi:10.1016/j.epsl.2016.04.013

19. K. Pahnke, R. Zahn, H. Elderfield, M. Schulz, 340,000-year centennial-scale marine record of Southern Hemisphere climatic oscillation. *Science* **301**, 948–952 (2003). doi:10.1126/science.1084451 Medline

20. K. Pahnke, R. Zahn, Southern Hemisphere water mass conversion linked with North Atlantic climate variability. *Science* **307**, 1741–1746 (2005). doi:10.1126/science.1102163 Medline

21. G. Siani, E. Michel, R. De Pol-Holz, T. Devries, F. Lamy, M. Carel, G. Isguder, F. Dewilde, A. Lourantou, Carbon isotope records reveal precise timing of enhanced Southern Ocean upwelling during the last deglaciation. *Nat. Commun.* **4**, 2758 (2013). doi:10.1038/ncomms3758 Medline

22. N. L. Roberts, A. M. Piotrowski, J. F. McManus, L. D. Keigwin, Synchronous deglacial overturning and water mass source changes. *Science* **327**, 75–78 (2010). doi:10.1126/science.1178068 Medline

23. W. B. Curry, D. W. Oppo, Glacial water mass geometry and the distribution of $\delta^{13}C$ of ΣCO_2 in the western Atlantic Ocean. *Paleoceanography* **20**, PA1017 (2005). doi:10.1029/2004PA001021

24. J. N. W. Howe, A. M. Piotrowski, T. L. Noble, S. Mulitza, C. M. Chiessi, G. Bayon, North Atlantic Deep Water Production during the Last Glacial Maximum. *Nat. Commun.* **7**, 11765 (2016). doi:10.1038/ncomms11765 Medline

25. L. D. Keigwin, S. A. Swift, Carbon isotope evidence for a northern source of deep water in the glacial western North Atlantic. *Proc. Natl. Acad. Sci. U.S.A.* **114**, 2831–2835 (2017). doi:10.1073/pnas.1614693114 Medline

26. J. W. B. Rae, M. Sarnthein, G. L. Foster, A. Ridgwell, P. M. Grootes, T. Elliott, Deep water formation in the North Pacific and deglacial CO_2 rise. *Paleoceanography* **29**, 645–667 (2014). doi:10.1002/2013PA002570

27. I. R. Hall, I. N. McCave, N. J. Shackleton, G. P. Weedon, S. E. Harris, Intensified deep Pacific inflow and ventilation in Pleistocene glacial times. *Nature* **412**, 809–812 (2001). doi:10.1038/35090552 Medline

28. J. F. Adkins, The role of deep ocean circulation in setting glacial climates. *Paleoceanography* **28**, 539–561 (2013). doi:10.1002/palo.20046

29. J. F. Adkins, K. McIntyre, D. P. Schrag, The salinity, temperature, and $\delta^{18}O$ of the glacial deep ocean. *Science* **298**, 1769–1773 (2002). doi:10.1126/science.1076252 Medline

30. F. Lamy, H. W. Arz, R. Kilian, C. B. Lange, L. Lembke-Jene, M. Wengler, J. Kaiser, O. Baeza-Urrea, I. R. Hall, N. Harada, R. Tiedemann, Glacial reduction and millennial-scale variations in Drake Passage throughflow. *Proc. Natl. Acad. Sci. U.S.A.* **112**, 13496–13501 (2015). doi:10.1073/pnas.1509203112 Medline

31. M. Nikurashin, R. Ferrari, Overturning circulation driven by breaking internal waves in the deep ocean. *Geophys. Res. Lett.* **40**, 3133–3137 (2013). doi:10.1002/grl.50542

32. L. C. Skinner, S. Fallon, C. Waelbroeck, E. Michel, S. Barker, Ventilation of the deep Southern Ocean and deglacial CO2 rise. *Science* **328**, 1147–1151 (2010). doi:10.1126/science.1183627 Medline

33. A. M. Piotrowski, S. L. Goldstein, S. R. Hemming, R. G. Fairbanks, Temporal relationships of carbon cycling and ocean circulation at glacial boundaries. *Science* **307**, 1933–1938 (2005). doi:10.1126/science.1104883 Medline

34. J. Lynch-Stieglitz, J. F. Adkins, W. B. Curry, T. Dokken, I. R. Hall, J. C. Herguera, J. J.-M. Hirschi, E. V. Ivanova, C. Kissel, O. Marchal, T. M. Marchitto, I. N. McCave, J. F. McManus, S. Mulitza, U. Ninnemann, F. Peeters, E.-F. Yu, R. Zahn, Atlantic meridional overturning circulation during the Last Glacial Maximum. *Science* **316**, 66–69 (2007). doi:10.1126/science.1137127 Medline

35. J. R. Toggweiler, B. Samuels, Effect of drake passage on the global thermohaline circulation. *Deep Sea Res. Part I Oceanogr. Res. Pap.* **42**, 477–500 (1995). doi:10.1016/0967-0637(95)00012-U

36. L. Talley, Closure of the global overturning circulation through the Indian, Pacific, and Southern Oceans: Schematics and transports. *Oceanography (Wash. D.C.)* **26**, 80–97 (2013). doi:10.5670/oceanog.2013.07

37. S. Barker, G. Knorr, M. J. Vautravers, P. Diz, L. C. Skinner, Extreme deepening of the Atlantic overturning circulation during deglaciation. *Nat. Geosci.* **3**, 567–571 (2010). doi:10.1038/ngeo921

38. A. M. Piotrowski, A. Galy, J. A. L. Nicholl, N. Roberts, D. J. Wilson, J. A. Clegg, J. Yu, Reconstructing deglacial North and South Atlantic deep water sourcing using foraminiferal Nd isotopes. *Earth Planet. Sci. Lett.* **357-358**, 289–297 (2012). doi:10.1016/j.epsl.2012.09.036

39. T. van de Flierdt, L. F. Robinson, J. F. Adkins, S. R. Hemming, S. L. Goldstein, Temporal stability of the neodymium isotope signature of the Holocene to glacial North Atlantic. *Paleoceanography* **21**, (2006). doi:10.1029/2006PA001294

40. G. L. Foster, D. Vance, J. Prytulak, No change in the neodymium isotope composition of deep water exported from the North Atlantic on glacial-interglacial time scales. *Geology* **35**, 37–40 (2007). doi:10.1130/G23204A.1

41. L. C. Skinner, C. Waelbroeck, A. E. Scrivner, S. J. Fallon, Radiocarbon evidence for alternating northern and southern sources of ventilation of the deep Atlantic carbon pool during the last deglaciation. *Proc. Natl. Acad. Sci. U.S.A.* **111**, 5480–5484 (2014). doi:10.1073/pnas.1400668111 Medline

42. F. Lamy, D. Hebbeln, G. Wefer, High-resolution marine record of climatic change in mid-latitude chile during the last 28,000 years based on terrigenous sediment parameters. *Quat. Res.* **51**, 83–93 (1999). doi:10.1006/qres.1998.2010

43. J. R. Toggweiler, J. L. Russell, S. R. Carson, Midlatitude westerlies, atmospheric CO2, and climate change during the ice ages. *Paleoceanography* **21**, n/a (2006). doi:10.1029/2005PA001154

44. E. L. Sikes, A. C. Elmore, K. A. Allen, M. S. Cook, T. P. Guilderson, Glacial water mass structure and rapid $\delta^{18}O$ and $\delta^{13}C$ changes during the last glacial termination in the Southwest Pacific. *Earth Planet. Sci. Lett.* **456**, 87–97 (2016). doi:10.1016/j.epsl.2016.09.043

45. H. E. Garcia *et al.*, *World Ocean Atlas 2009, NOAA Atlas No. NESDros. Inf. Serv. 70* (NOAA, 2010).

46. J. I. Antonov *et al.*, *World Ocean Atlas 2009, NOAA Atlas No. NESDros. Inf. Serv. 69* (NOAA, 2010).

47. A. H. Orsi, T. Whitworth III, W. D. Nowlin Jr., On the meridional extent and fronts of the Antarctic Circumpolar Current. *Deep Sea Res. Part I Oceanogr. Res. Pap.* **42**, 641–673 (1995). doi:10.1016/0967-0637(95)00021-W

48. P. Grootes, M. Stuiver, Oxygen 18/16 variability in Greenland snow and ice with 10^{-3} to 10^{5} year time resolution. *J. Geophys. Res.* **102** (C12), 26455–26470 (1997). doi:10.1029/97JC00880

49. J. Jouzel, V. Masson-Delmotte, O. Cattani, G. Dreyfus, S. Falourd, G. Hoffmann, B. Minster, J. Nouet, J. M. Barnola, J. Chappellaz, H. Fischer, J. C. Gallet, S. Johnsen, M. Leuenberger, L. Loulergue, D. Luethi, H. Oerter, F. Parrenin, G. Raisbeck, D. Raynaud, A. Schilt, J. Schwander, E. Selmo, R. Souchez, R. Spahni, B. Stauffer, J. P. Steffensen, B. Stenni, T. F. Stocker, J. L. Tison, M. Werner, E. W. Wolff, Orbital and millennial Antarctic climate variability over the past 800,000 years. *Science* **317**, 793–796 (2007). doi:10.1126/science.1141038 Medline

50. D. Veres, L. Bazin, A. Landais, H. Toyé Mahamadou Kele, B. Lemieux-Dudon, F. Parrenin, P. Martinerie, E. Blayo, T. Blunier, E. Capron, J. Chappellaz, S. O. Rasmussen, M. Severi, A. Svensson, B. Vinther, E. W. Wolff, The Antarctic ice core chronology (AICC2012): An optimized multi-parameter and multi-site dating approach for the last 120 thousand years. *Clim. Past* **9**, 1733–1748 (2013). doi:10.5194/cp-9-1733-2013

51. WAIS Divide Project Members, Onset of deglacial warming in West Antarctica driven by local orbital forcing. *Nature* **500**, 440–444 (2013). doi:10.1038/nature12376 Medline

52. E. Monnin, A. Indermühle, A. Dällenbach, J. Flückiger, B. Stauffer, T. F. Stocker, D. Raynaud, J. M. Barnola, Atmospheric CO_2 concentrations over the last glacial termination. *Science* **291**, 112–114 (2001). doi:10.1126/science.291.5501.112 Medline

53. R. Gersonde, “The expedition of the research vessel “Polarstern” to the polar South Pacific in 2009/2010 (ANT-XXVI/2 - BIPOMAC)” (Alfred Wegener Institute for Polar and Marine Research, Bremerhaven, (2011)).

54. K. Tachikawa, A. M. Piotrowski, G. Bayon, Neodymium associated with foraminiferal carbonate as a recorder of seawater isotopic signatures. *Quat. Sci. Rev.* **88**, 1–13 (2014). doi:10.1016/j.quascirev.2013.12.027

55. C. Pin, J. S. Zalduegui, Sequential separation of light rare-earth elements, thorium and uranium by miniaturized extraction chromatography: Application to isotopic analyses of silicate rocks. *Anal. Chim. Acta* **339**, 79–89 (1997). doi:10.1016/S0003-2670(96)00499-0

56. R. K. O’Nions, P. J. Hamilton, N. M. Evensen, Variations in143Nd/144Nd and87Sr/86Sr ratios in oceanic basalts. *Earth Planet. Sci. Lett.* **34**, 13–22 (1977). doi:10.1016/0012-821X(77)90100-5

57. T. Tanaka, S. Togashi, H. Kamioka, H. Amakawa, H. Kagami, T. Hamamoto, M. Yuhara, Y. Orihashi, S. Yoneda, H. Shimizu, T. Kunimaru, K. Takahashi, T. Yanagi, T. Nakano, H. Fujimaki, R. Shinjo, Y. Asahara, M. Tanimizu, C. Dragusanu, JNdi-1: A neodymium isotopic reference in consistency with LaJolla neodymium. *Chem. Geol.* **168**, 279–281 (2000). doi:10.1016/S0009-2541(00)00198-4

58. P. J. Reimer, E. Bard, A. Bayliss, J. W. Beck, P. G. Blackwell, C. B. Ramsey, C. E. Buck, H. Cheng, R. L. Edwards, M. Friedrich, P. M. Grootes, T. P. Guilderson, H. Haflidason, I. Hajdas, C. Hatté, T. J. Heaton, D. L. Hoffmann, A. G. Hogg, K. A. Hughen, K. F. Kaiser, B. Kromer, S. W. Manning, M. Niu, R. W. Reimer, D. A. Richards, E. M. Scott, J. R. Southon, R. A. Staff, C. S. M. Turney, J. van der Plicht, IntCal13 and Marine13 radiocarbon age calibration curves 0–50,000 years cal BP. *Radiocarbon* **55**, 1869–1887 (2013). doi:10.2458/azu_js_rc.55.16947

59. E. L. Sikes, C. R. Samson, T. P. Guilderson, W. R. Howard, Old radiocarbon ages in the southwest Pacific Ocean during the last glacial period and deglaciation. *Nature* **405**, 555–559 (2000). doi:10.1038/35014581 Medline

60. K. A. Rose, E. L. Sikes, T. P. Guilderson, P. Shane, T. M. Hill, R. Zahn, H. J. Spero, Upper-ocean-to-atmosphere radiocarbon offsets imply fast deglacial carbon dioxide release. *Nature* **466**, 1093–1097 (2010). doi:10.1038/nature09288 Medline

61. M. J. Vandergoes, A. G. Hogg, D. J. Lowe, R. M. Newnham, G. H. Denton, J. Southon, D. J. A. Barrell, C. J. N. Wilson, M. S. McGlone, A. S. R. Allan, P. C. Almond, F. Petchey, K. Dabell, A. C. Dieffenbacher-Krall, M. Blaauw, A revised age for the Kawakawa/Oruanui tephra, a key marker for the Last Glacial Maximum in New Zealand. *Quat. Sci. Rev.* **74**, 195–201 (2013). doi:10.1016/j.quascirev.2012.11.006

62. D. Paillard, L. Labeyrie, P. Yiou, Macintosh program performs time-series analysis. *Eos (Wash. D.C.)* **77**, 379–379 (1996). doi:10.1029/96EO00259

63. F. Lamy, R. Gersonde, G. Winckler, O. Esper, A. Jaeschke, G. Kuhn, J. Ullermann, A. Martinez-Garcia, F. Lambert, R. Kilian, Increased dust deposition in the Pacific Southern Ocean during glacial periods. *Science* **343**, 403–407 (2014). doi:10.1126/science.1245424 Medline

64. V. Benz, O. Esper, R. Gersonde, F. Lamy, R. Tiedemann, Last Glacial Maximum sea surface temperature and sea-ice extent in the Pacific sector of the Southern Ocean. *Quat. Sci. Rev.* **146**, 216–237 (2016). doi:10.1016/j.quascirev.2016.06.006

65. A. S. Studer, D. M. Sigman, A. Martínez-García, V. Benz, G. Winckler, G. Kuhn, O. Esper, F. Lamy, S. L. Jaccard, L. Wacker, S. Oleynik, R. Gersonde, G. H. Haug, Antarctic Zone nutrient conditions during the last two glacial cycles. *Paleoceanography* **30**, 845–862 (2015). doi:10.1002/2014PA002745

66. U. S. Ninnemann, C. D. Charles, Changes in the mode of Southern Ocean circulation over the last glacial cycle revealed by foraminiferal stable isotopic variability. *Earth Planet. Sci. Lett.* **201**, 383–396 (2002). doi:10.1016/S0012-821X(02)00708-2

67. B. M. Sloyan, S. R. Rintoul, Circulation, renewal, and modification of Antarctic mode and intermediate water. *J. Phys. Oceanogr.* **31**, 1005–1030 (2001). doi:10.1175/1520-0485(2001)031<1005:CRAMOA>2.0.CO;2

68. J. L. Reid, R. J. Lynn, On the influence of the Norwegian-Greenland and Weddell seas upon the bottom waters of the Indian and Pacific oceans. *Deep-Sea Res.* **18**, 1063–1088 (1971).

69. J. E. Callahan, The structure and circulation of deep water in the Antarctic. *Deep-Sea Res. Oceanogr. Abstr.* **19**, 563–575 (1972). doi:10.1016/0011-7471(72)90040-X

70. M. Kawabe, S. Fujio, Pacific ocean circulation based on observation. *J. Oceanogr.* **66**, 389–403 (2010). doi:10.1007/s10872-010-0034-8

71. A. H. Orsi, G. C. Johnson, J. L. Bullister, Circulation, mixing, and production of Antarctic Bottom Water. *Prog. Oceanogr.* **43**, 55–109 (1999). doi:10.1016/S0079-6611(99)00004-X

72. S. B. Jacobsen, G. J. Wasserburg, Sm-Nd isotopic evolution of chondrites. *Earth Planet. Sci. Lett.* **50**, 139–155 (1980). doi:10.1016/0012-821X(80)90125-9

73. C. Jeandel, T. Arsouze, F. Lacan, P. Techine, J. Dutay, Isotopic Nd compositions and concentrations of the lithogenic inputs into the ocean: A compilation, with an emphasis on the margins. *Chem. Geol.* **239**, 156–164 (2007). doi:10.1016/j.chemgeo.2006.11.013

74. K. Tachikawa, V. Athias, C. Jeandel, Neodymium budget in the modern ocean and paleo-oceanographic implications. *J. Geophys. Res. Oceans* **108** (C8), 3254 (2003). doi:10.1029/1999JC000285

75. J. Rempfer, T. F. Stocker, F. Joos, J.-C. Dutay, M. Siddall, Modelling Nd-isotopes with a coarse resolution ocean circulation model: Sensitivities to model parameters and source/sink distributions. *Geochim. Cosmochim. Acta* **75**, 5927–5950 (2011). doi:10.1016/j.gca.2011.07.044

76. S. L. Goldstein, S. H. Hemming, in *Treatise on Geochemistry*, H. Elderfield, Ed. (Elsevier, 2003), pp. 453–489.

77. F. Lacan, C. Jeandel, Tracing Papua New Guinea imprint on the central Equatorial Pacific Ocean using neodymium isotopic compositions and Rare Earth Element patterns. *Earth Planet. Sci. Lett.* **186**, 497–512 (2001). doi:10.1016/S0012-821X(01)00263-1

78. P. Carter, D. Vance, C. D. Hillenbrand, J. A. Smith, D. R. Shoosmith, The neodymium isotopic composition of waters masses in the eastern Pacific sector of the Southern Ocean. *Geochim. Cosmochim. Acta* **79**, 41–59 (2012). doi:10.1016/j.gca.2011.11.034

79. J. Rickli, M. Gutjahr, D. Vance, M. Fischer-Gödde, C.-D. Hillenbrand, G. Kuhn, Neodymium and hafnium boundary contributions to seawater along the West Antarctic continental margin. *Earth Planet. Sci. Lett.* **394**, 99–110 (2014). doi:10.1016/j.epsl.2014.03.008

80. M. Molina-Kescher, M. Frank, E. Hathorne, South Pacific dissolved Nd isotope compositions and rare earth element distributions: Water mass mixing versus biogeochemical cycling. *Geochim. Cosmochim. Acta* **127**, 171–189 (2014). doi:10.1016/j.gca.2013.11.038

81. W. Abouchami, S. L. Goldstein, S. J. G. Gazer, A. Eisenhauer, A. Mangini, Secular changes of lead and neodymium in central Pacific seawater recorded by a Fe-Mn crust. *Geochim. Cosmochim. Acta* **61**, 3957–3974 (1997). doi:10.1016/S0016-7037(97)00218-4

82. T. M. Marchitto, J. Lynch-Stieglitz, S. R. Hemming, Deep Pacific $CaCO_3$ compensation and glacial–interglacial atmospheric CO_2. *Earth Planet. Sci. Lett.* **231**, 317–336 (2005). doi:10.1016/j.epsl.2004.12.024

83. F. Lacan, C. Jeandel, Neodymium isotopic composition and rare earth element concentrations in the deep and intermediate Nordic Seas: Constraints on the Iceland Scotland Overflow Water signature. *Geochem. Geophys. Geosyst.* **5**, Q11006 (2004). doi:10.1029/2004GC000742

84. E. E. Martin, B. A. Haley, Fossil fish teeth as proxies for seawater Sr and Nd isotopes. *Geochim. Cosmochim. Acta* **64**, 835–847 (2000). doi:10.1016/S0016-7037(99)00376-2

85. E. E. Martin, S. W. Blair, G. D. Kamenov, H. D. Scher, E. Bourbon, C. Basak, D. N. Newkirk, Extraction of Nd isotopes from bulk deep sea sediments for paleoceanographic studies on Cenozoic time scales. *Chem. Geol.* **269**, 414–431 (2010). doi:10.1016/j.chemgeo.2009.10.016

86. K. Pahnke, S. L. Goldstein, S. R. Hemming, Abrupt changes in Antarctic Intermediate Water circulation over the past 25,000 years. *Nat. Geosci.* **1**, 870–874 (2008). doi:10.1038/ngeo360

87. A. N. Abbott, B. A. Haley, J. McManus, Bottoms up: Sedimentary control of the deep North Pacific Ocean's ε_{Nd} signature. *Geology* **43**, 1035–1038 (2015). doi:10.1130/G37114.1

88. D. J. Thomas, R. K. Via, Neogene evolution of atlantic thermohaline circulation: Perspective from Walvis Ridge, southeastern Atlantic Ocean. *Paleoceanography* **22**, PA2212 (2007). doi:10.1029/2006PA001297

89. A. C. Elmore, A. M. Piotrowski, J. D. Wright, A. E. Scrivner, Testing the extraction of past seawater Nd isotopic composition from North Atlantic deep sea sediments and

foraminifera. *Geochem. Geophys. Geosyst.* **12**, Q09008 (2011). doi:10.1029/2011GC003741

90. G. Charbonnier, E. Pucéat, G. Bayon, D. Desmares, G. Dera, C. Durlet, J.-F. Deconinck, F. Amédro, A. T. Gourlan, P. Pellenard, B. Bomou, Reconstruction of the Nd isotope composition of seawater on epicontinental seas: Testing the potential of Fe–Mn oxyhydroxide coatings on foraminifera tests for deep-time investigations. *Geochim. Cosmochim. Acta* **99**, 39–56 (2012). doi:10.1016/j.gca.2012.09.012

91. R. Schlitzer, Ocean data view (2014); http://odv.awi.de.